International Journal of Engineering Trends and Technology
ISSN: 2231 – 5381 / https://doi.org/10.14445/22315381/IJETT-V71I1P215

Volume 71 Issue 1, 164-177, January 2023

Original Article

Design and Performance Analysis of Five-Phase Fault-Tolerant Spoke-Type PM Motor with Two Distinctive Rotor Topology for Electric Vehicle Traction Application

Stephen Eduku[1], Joseph Sekyi-Ansah[2], Mohammed Okoe Alhassan[3], Ebenezer Narh Odonkor[1]

[1] *Department of Electrical and Electronics Engineering, Takoradi Technical University, Takoradi, Ghana.*
[2,3] *Department of Mechanical Engineering, Takoradi Technical University, Takoradi, Ghana.*

[1]*Corresponding Author: 5103180335@stmail.ujs.edu.cn*

Received: 25 November 2022 Revised: 12 January 2023 Accepted: 15 January 2023 Published: 24 January 2023

Abstract *- In this paper, a five-phase fault-tolerant spoke-type permanent magnet (PM) motor with two distinctive rotor topologies is designed and analyzed for electric vehicles (EV). Meanwhile, the designed topologies considered in this paper are classified according to the rotor topology. They are termed the modular rotor spoke-type PM (MRSTPM) motor and the union rotor spoke-type PM (URSTPM) motor. However, for fair and comprehensive performance analysis, the same design specifications, such as the PM volume, rotor and stator dimensions, slot-pole combination, and winding arrangement, are adopted for both topologies. The electromagnetic performances of the two topologies with their static characteristics, namely, the flux-linkage, back-EMF, cogging-torque, output-torque, losses, and torque-ripple, are analyzed to unveil the opportunities and limitations of the motors. Moreover, the electromagnetic performances of both topologies are analyzed and compared using the finite element analysis (FEA) principle. However, the obtained results depict that the MRSTPM-motor exhibit slightly higher output-toque, power density, and torque density than the URSTPM-motor. Nonetheless, it is imperative to highlight that the URSTPM-motor is a promising design candidate for an electric vehicle (EV) traction application. It unveils an enhanced fault-tolerant capacity, reduced cogging torque, lower torque ripple, minimal motor losses, and higher efficiency compared to the MRSTPM-motor topology. Besides, the URSTPM-motor has the additional merit of easy rotor construction compared to the MRSTPM-motor topology.*

Keywords *- Spoke-Type PM motor, Fault-Tolerant, Finite Element Analysis (FEA), Electric Vehicle (EV).*

1. Introduction

The state of environmental pollution and the scarcity of various forms of energy across the globe in recent years have inevitably attracted in-depth and extensive research enthusiasm into electric vehicles (EVs) and hybrid electric vehicles (HEVs) traction [1-3]. Besides, EV and HEV traction applications require electrical-designed motors with a higher exhibition of electromagnetic output torque and higher output torque density during the operating condition, which has been recognized as an inevitable design challenge [4]. Moreover, an electrical motor with higher power density production capacity is imperative or key, owing to space constraints and the miniaturization of modern technological advancement across the globe. Motor efficiency in EV and HEV applications is a key concern as it saves energy and increases the range of driving per charge. Meanwhile, permanent magnet motors have high torque density and high operating efficiency in low-speed regions and are extensively employed in electric vehicles and hybrid electric vehicles [5].

Nevertheless, the permanent magnet (PM) brushless motors provide higher power density and operating efficiency, making them an attractive and promising candidate in EV and HEV applications, just like the Toyota Prius motors [6-10]. However, PM brushless-designed motors do away with excitation windings to unveil a higher torque density, higher power density, and higher-operating efficiency [11] and [12]. Besides, PM-designed motors are successfully and vastly employed in EVs, HEVs, electric aircraft (EA), and other key industrial applications [13-16].

Meanwhile, considering the PM-designed motor categories, the spoke-type PM-designed motors exhibit an improved air-gap distributed flux-density, owing to its flux concentrating or focusing effect produced by the two adjacent positioned PMs, thus, resulting in higher torque-density production with corresponding inherent PM savings. Besides, it is imperative to highlight that the spoke-type PM-designed motors unearth a serious demerit by exhibiting a

serious distortion in the distribution of the air-gap flux density, hence, giving rise to various harmonic orders in the generated back electromotive force, higher-torque ripple, or pulsation, and higher cogging-torque [16-20]. Nonetheless, the above-mentioned demerit has the potential to emit or induce an undesirable vibration with a corresponding high acoustic noise level, with sequence influence on the motor mounting position, which may affect the operating performance of the motor [43].

Furthermore, special design characteristics of electrical motors, such as higher torque production abilities, minimal torque pulsations, great overload capacity, and higher running efficiency, are greatly anticipated and desirable in EV traction applications [22-24]. Besides, in-depth research in switched reluctance designed motors with an emphasis on higher output performances in an aerospace application has attracted great attention due to its inherent fault-tolerant property. However, recent research unveils or predicts that, with meticulous design measures, permanent magnet-designed motors can exhibit an identical degree of fault-tolerant with higher output torque density compared to the switched reluctance (SR) design motor counterpart [25-30].

However, implementing fault-tolerant technology in electrical rotating machines presents a higher degree of freedom in fault conditions such as open and short-circuit in single or double-phase windings compared to the three-phase design machine topologies. Nevertheless, from the analysis mentioned above, this research aims at design and performance comparison analysis of a five-phase fault-tolerant spoke-type permanent magnet motor with two distinctive rotor-topology to ascertain the topology which not only minimized the above-mentioned issues or demerits in the spoke-type permanent magnet motor; but also exhibits an enhanced or higher electromagnetic output performance such as power density, torque density, operating efficiency, output torque, and minimal PM and core losses with an excellent fault-tolerant capacity.

2. Motor Topologies Design Analysis

The design topologies of both the MRSTPM motor and the URSTPM motor are presented in Fig.1 (a) and (b), respectively. However, as illustrated in Fig.1 (a), the MRSTPM motor, as the name implies, has its rotor topology configured with separate rotor cells as compared to the URSTPM motor with a one-complete or integrated rotor-topology as depicted in Fig. 1(b). Hence, constructing the MRSTPM motor complex compared to the URSTPM motor. Besides, in [31], modular and integrated designed rotor topologies of PM motors are comprehensively studied, and the outcome of the manufacturability analysis depicts that PM motors with an integrated or union rotor have easy manufacturability compared to the PM motors which incorporate modular or segregated rotor designed topologies.

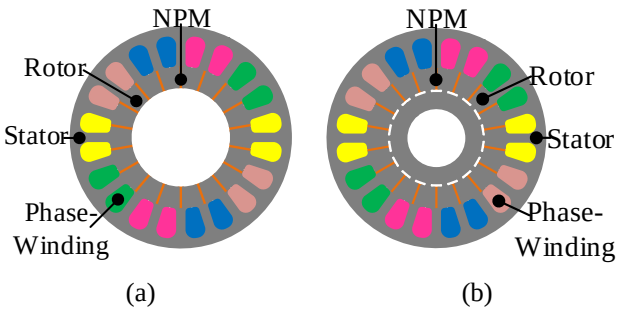

Fig. 1 Topologies of the spoke-type PM motors. (a) MRSTPM- Motor. (b) URSTPM-Motor

Table 1. Key Design Parameters Specifications of Both Topologies

Items	MRSTPM-Motor	URSTPM-Motor
Number of stator slot/rotor pole	20/18	20/18
Number of turns per-slot	35	35
Rated speed (r/min)	1500	1500
Rated current (A)	8.2	8.2
Active axial length (mm)	60	60
Stator outer diameter (mm)	145	145
Stator inner diameter (mm)	92.7	92.7
Air-gap length (mm)	0.5	0.5
Rotor outer diameter (mm)	91.7	91.7
Rotor inner diameter (mm)	25	25
Iron core material	DW540_50	DW540_50
PM volume (mm^3)	2241.6	2241.6
PM material	NdFe35	NdFe35
Remanence of PM (T)	1.23	1.23

Moreover, it is imperative to highlight that both motors have the same design material specifications, such as stator-rotor dimensions, slot-pole combination, PM-Volume, laminated core, and winding configuration. Nonetheless, for intuitive analysis, the aforementioned design material specifications are presented in Table 1.

3. Slot-Pole Synergy and Winding Analysis

The stator-slot and rotor-pole synergy of an electrical rotating machine (motor) is a fundamental and critical design component to study at the initial or prefatory design stage to ensure a higher main harmonic winding factor (kwm), to achieve a torque density and power density and to ascertain higher least common multiple (LCM) of stator-slots (*Qs*). The number of rotor-poles (*2Pr*) ensures a minimal cogging torque to avert acoustic noise and vibration, which can lead to poor motor positioning. Finally, obtain an even number and a higher greatest common divisor (GCD) of the *Qs* and *2Pr* to ensure balanced magnetic radial forces (BMRFs) with an enhanced radial symmetry of the design. Howbeit, an electrical motor with fractional-slot concentrated winding configurations (FSCWCs), designed to satisfy the condition or design specification *2Pr = Qs±2*, can exhibit an enhanced torque density and power density, which is pretty meritorious or worthy for EV tractions application.

In the modular winding configuration of PM motors with a stipulated number of phases (m) and *Qs*, the recommended *2Pr* and its corresponding angle measured between two adjacent design slots can be computed via equations (1) and (2), respectively.

$$2\,\mathrm{P_r} = Q_s\left[1 \pm {}^{k}\!/_{2m}\right] \tag{1}$$

$$\theta_s = 2\pi\left[1 \pm {}^{k}\!/_{2m}\right] \tag{2}$$

Where the parameter *k*=1 or the selected design values. Besides, the value *k* can be any old number that is a nonzero integer but less than the value m to satisfy a design condition, such that the two quantities, namely, *k* and m, don't share any specific common factors. Moreover, for a multiphase motor with m=5, the corresponding values of k can be 1 and 3, respectively. This paper's design specification for the Spoke-Type PM motor is 20-laminated stator slots to be supplied via a 5-phase full-bridge or H-Type converter. Hence, computing the required rotor-pole number with the k and m values using equations (1) and (2), respectively, are depicted as follows:

- For the value *k=1*, the required *2P=18* is the low value, and *2P=22* is the high value with the corresponding computed phase angle of 36^0 in the clockwise direction and -36^0 in the anticlockwise direction measured between the designated phases.
- For the value *k=3*, the requisite *2P=14* represents the low value and *2P=26* depicts the high value with the corresponding computed phase angle between the designated phases being 108^0 in the clockwise direction and -108^0 in the anticlockwise direction.

In Table 2, it can be observed that the commonly employed stator slots (*Qs=20*) with *2P=18* and *2P=22* are the attractive synergy for the motor design. Nonetheless, the 20 stator-slots and 22 rotor-poles synergy exhibit a higher winding factor to enhance the electromagnetic torque and higher LCM, making it a promising design candidate for minimizing the cogging-torque and torque-ripple, which is key in EV traction applications. Besides, it is imperative to highlight that a significant increase in the rotor-poles requires a power electronics converter with higher operating or supply frequency, which unveils or introduces a manufacturing intricacy or complexity in terms of large-scale production. Hence, the 20 stator-slots and 18 rotor-poles synergies exhibit the same winding factor and also fulfill the design condition of *2p±2* to ensure a single-layer concentrated winding configuration to enhance the fault-tolerant capacity of the motor, and with the same electromagnet torque, compared with the 20 stator-slots, and 22 rotor-poles combinations are adopted in this paper. Nevertheless, an extensive detailed slot-pole synergy or combination analysis can be traced or established in [32-38].

Table 2. Slot- Pole Combination Analysis of both Topologies

Qs	*2Pr*	*2Pr = Qs±2*	SSP	LCM	GCD	Kwm
20	18	2	2/9	180	2	**0.9755**
	22	2	2/11	660	2	**0.9755**
20	14	-	2/7	140	2	0.8800
	26	-	2/13	260	2	0.8802

Besides, Fig. 2(a) and (b) respectively present the star of slots and winding connection of both topologies. Meanwhile, the established electrical angle (*αe*) obtained between two adjacent slot phasors of the stator can be computed by (3), and its corresponding angle established between two designed spokes (*αsp*) can be obtained via (4).

$$\alpha e = \frac{2\pi}{Q_S} \times P_r = 162^0 \tag{3}$$

$$\alpha_{sp} = \frac{\alpha e}{P_r} t = 36^0 \tag{4}$$

Where *t* and P_r depict motor-periodicity and rotor-pole pair number, respectively, the star of the slot of the topologies can be categorized into ten (2m) sectors and the corresponding computed span-angle of each designed sector is (2π/2m) degrees. However, two opposite-designed sectors are designated for each phase-winding, with two sectors marked as positive-terminals (A+) and the other two as negative-terminals (A-), as presented in the star of slots with the yellow colors in Fig.2(a). Besides, from the star of slots in Fig2, the aforementioned sectors are displaced with a displacement angle of 180 degrees. However, the five-phase winding sinusoidal and symmetrical injected-current of both topologies at the normal operating condition can be computed by the expression in (5). Moreover, the main winding *Kwm*, as presented in Table II, can be computed or established via the succeeding expression:

$$K_{wm} = K_d K_p \tag{4}$$

Where k_d denotes the distribution factor and the symbol *kp* depicts the pitch factor of the machine.

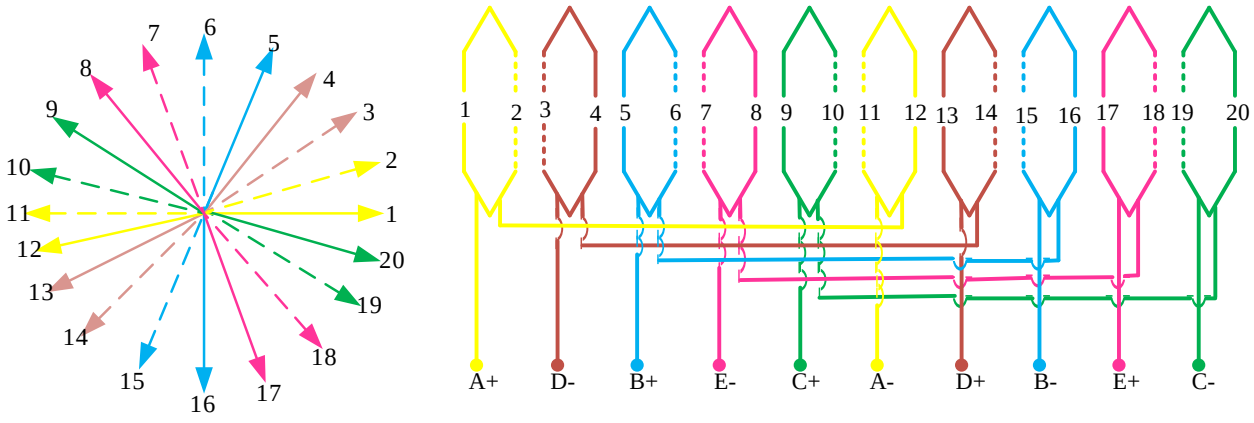

(a) **(b)**

Fig. 2 The 20-slot with an 18-pole combination Winding-Design Analysis for both spoke-type PM motors

$$\begin{cases} i_A = I_m \sin(\omega t) \\ i_B = I_m \sin(\omega t - 2\pi/5) \\ i_C = I_m \sin(\omega t - 4\pi/5) \\ i_D = I_m \sin(\omega t - 6\pi/5) \\ i_E = I_m \sin(\omega t - 8\pi/5) \end{cases} \quad (5)$$

Where the parameter I_m depicts the maximum phase current, and ωt represents the established angular speed measured in electrical degrees with respect to time.

4. Electromagnetic Performance Comparative Analysis of both Topologies

4.1. No-Load Design Performances Analysis

The key design characteristics of the no-load condition at an operating speed of 1500rpm analyzed in this section are the magnetic field distributions, flux-density distributions, air-gap flux density, flux-linkage, generated back electromotive-fore (black-EMF), and the obtained cogging-torque. Meanwhile, the above-mentioned design characteristics are chronologically arranged from Fig.3 to Fig.8. However, the open-circuit magnetic field flux-distributions of MSTPM-motor and USTPM-motor are presented respectively in Fig.3 (a) and (b) for intuitive analysis. Furthermore, it can be observed respectively in Fig.3 (a) and (b) that both topologies exhibit a comparative open-circuit field flux distribution. Moreover, Fig.4 (a) and (b) depict the flux-density distribution analysis of both topologies. Nonetheless, it is imperative to highlight that the MRSTPM-motor exhibits a slightly higher flux density as compared to the URSTPM-motor. Hence, for intuitive analysis, the peak values of the flux density of MRSTPM-motor and URSTPM-motor are 1.78T and 1.69T, respectively.

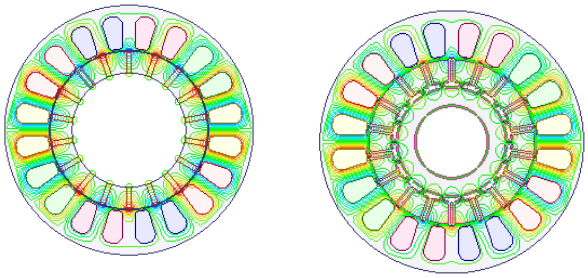

(a) **(b)**

Fig. 3 Magnetic field distribution of the spoke-type PM motors. (a) MRSTPM- Motor. (b) URSTPM-Motor

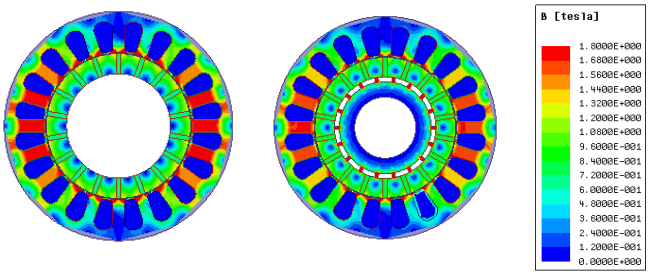

(a) **(b)** **(c)**

Fig. 4 Flux-density distribution of the spoke-type PM motors. (a) MRSTPM- Motor. (b) URSTPM-Motor

Fig.5 (a) and (b) depict the radial and tangential air-gap flux-density generated by both the MRSTPM-motor and URSTPM-Motor designs. As presented in Fig.5 (a) and (b), both topologies exhibit a comparative radial and tangential air-gap flux density. Hence, depicting the competitiveness between the MRSTPM-motor and the URSTPM-motor. Besides, to quantitatively buttress the aforementioned analysis, the computed air-gap flux density of the MRSTPM motor and that of the URSTPM motor topology are 1.52T and 1.26T, respectively.

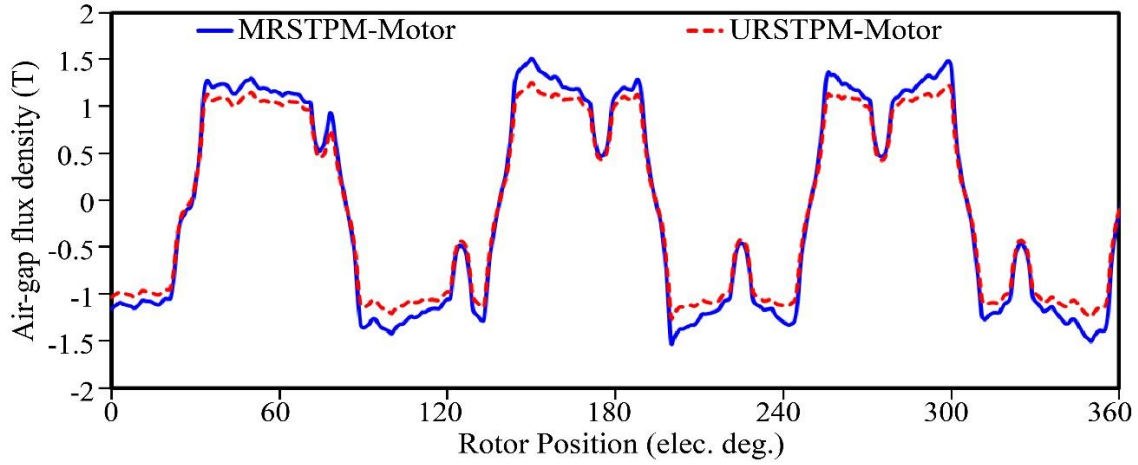

(a)

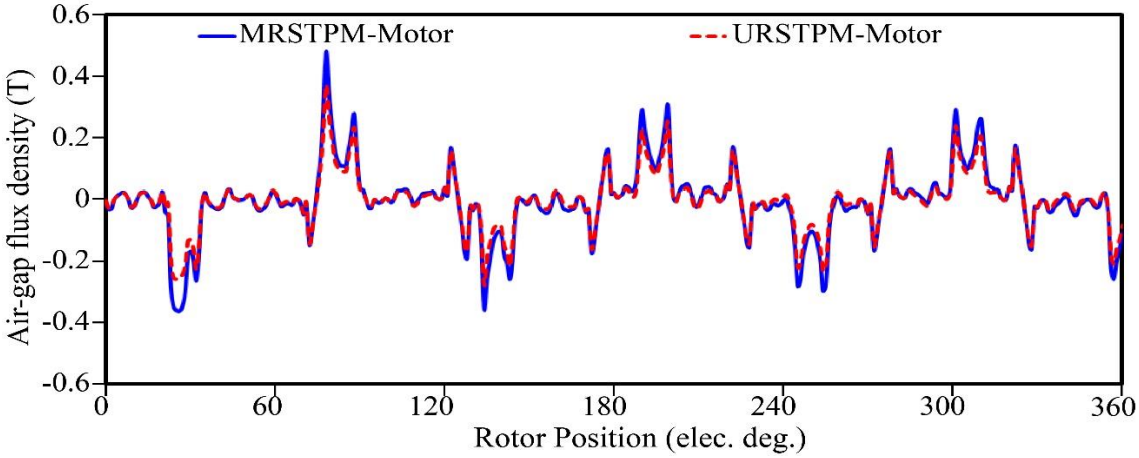

(b)

Fig. 5 Air-gap Flux-density distribution obtained by the spoke-type PM motors. (a) Radial-Flux-density along the air gap. (b) Tangential-Flux-density along the air gap

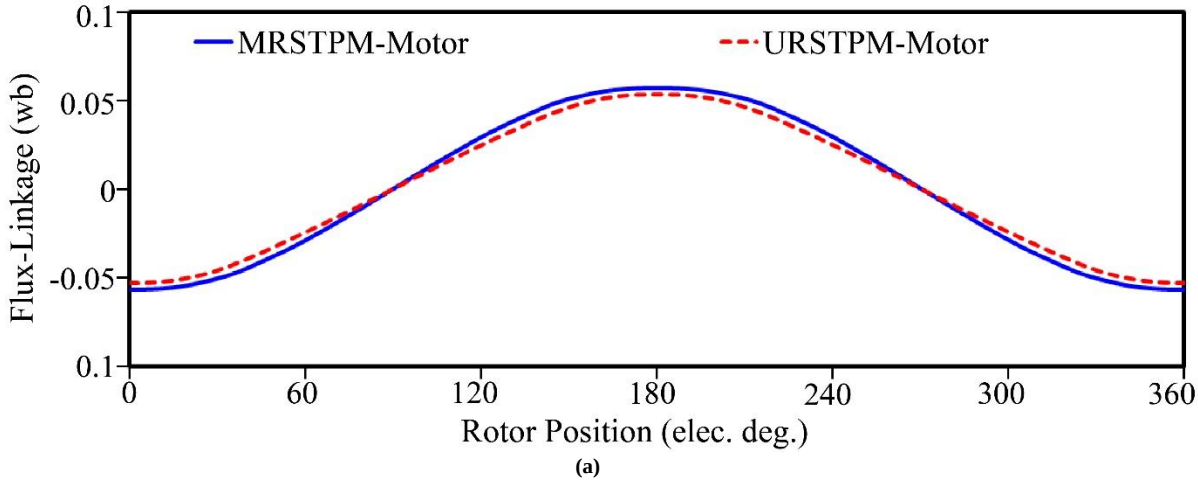

(a)

Fig. 6 (a) and (b) present the waveform of the phase-A flux-linkage and its harmonic order (harmonic spectrum), respectively. Meanwhile, as depicted in Fig.6(a), both the MRSTPM-motor and the URSTPM-motor unveil comparative phase-A flux-linkage waveforms. However, as shown in Fig.6 (b), the fundamental harmonic-order component of the MRSTPM-motor is slightly higher than that of the URSTPM-motor. Besides, the third harmonic order of the URSTPM-motor is higher than the MRSTPM-motor.

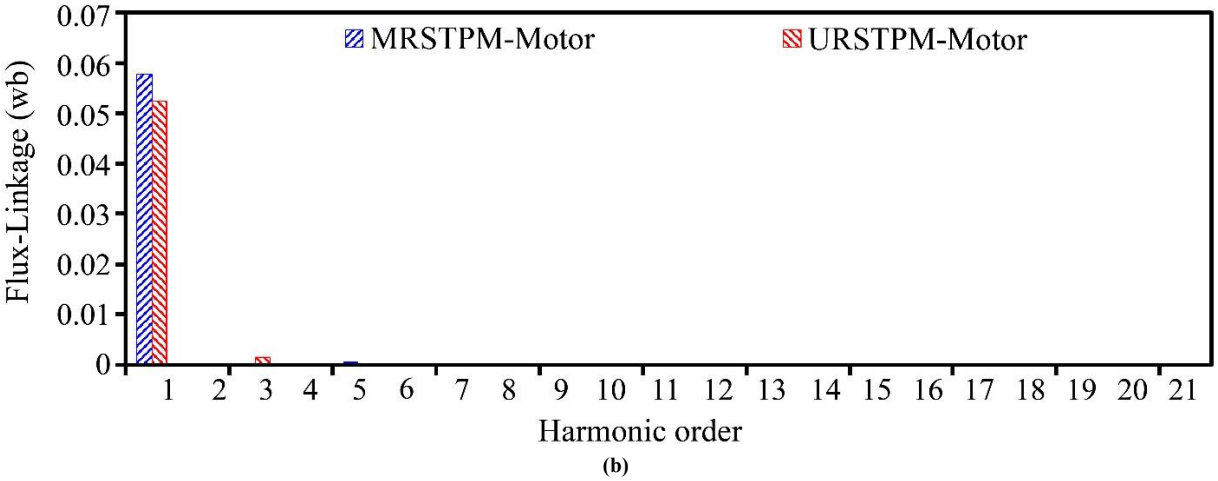

(b)

Fig. 6 Flux-Linkage obtained by the spoke-type PM motors. (a) waveforms. (b) Harmonic-order

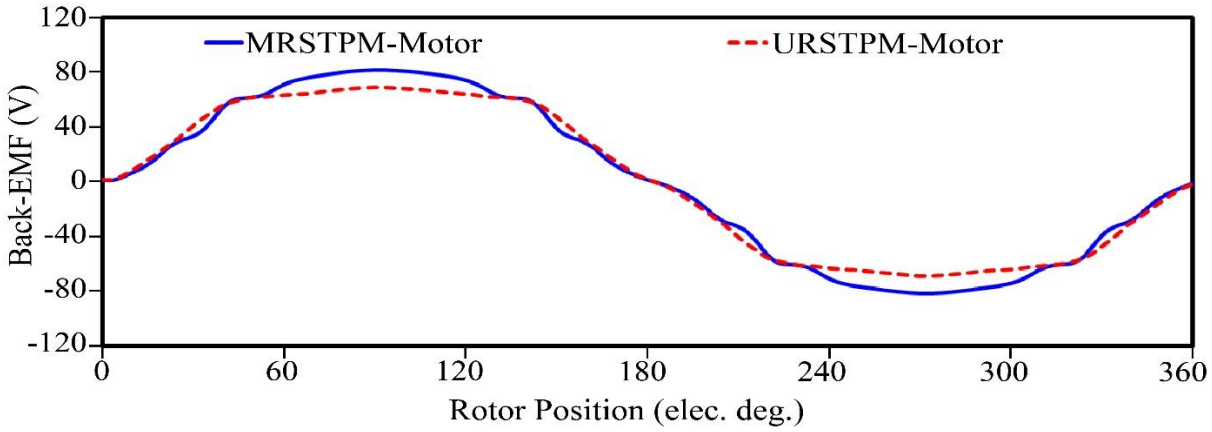

(a)

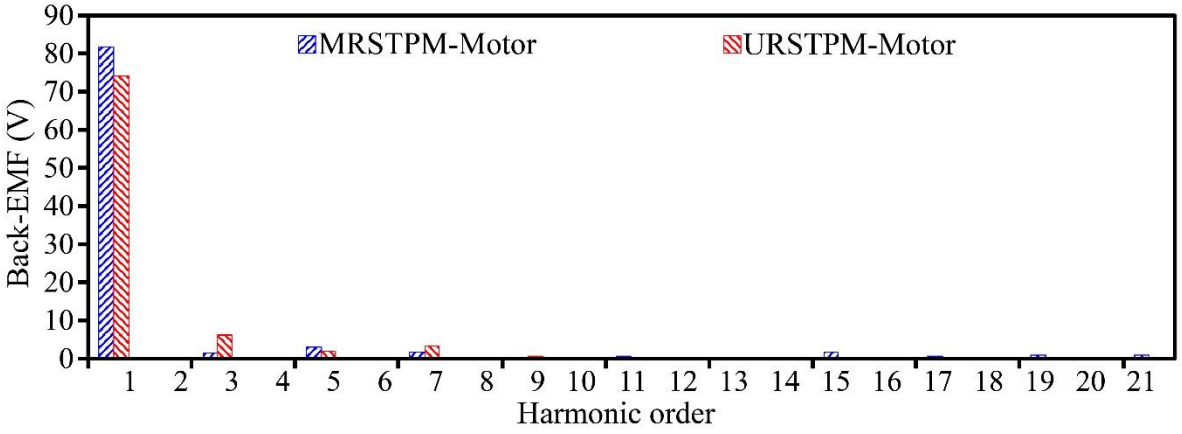

(b)

Fig. 7 No-Load back-EMF of the spoke-type PM motors at 1500 rpm. (a) Waveform (b) Harmonic orders

Fig.7 (a) and (b) illustrate the generated back-EMF waveforms and their associated harmonic order of both topologies. However, as presented in Fig.7(a), it is obvious that the MRSTPM-motor exhibits a higher back-EMF than the URSTPM-motor. Hence, it can be forecast, from an engineering point of view, that the MRSTPM-motor may unveil a higher output torque as compared to the URSTPM-motor. Moreover, as depicted in Fig.7(b), the MRSTPM-motor exhibit a higher fundamental component and 5th harmonic, with lower 3rd and 7th harmonic order than the URSTPM-motor. However, it is imperative to highlight that the key harmonic orders in the back-EMF of a poly-phase

motor (5-phase motor), such as the 9th, 11th, 19th, and 21st that have been unveiled or established to interact with the sinusoidal induced phase-current to produce torque-ripple or pulsations in the five-phase motor are infinitesimal or negligible in both topologies considered in this paper, as presented in Fig.7 (b). Besides, the total harmonics distortions (THDs) in the back-EMF can be derived from (6). Hence, the computed THD of the generated back-EMF for both the MRSTPM-motor and the URSTPM-motor is 5.4% and 6.5%, respectively.

$$THD = \frac{\sqrt{\sum_{i=2}^{\infty} Ei^{2}}}{E_1} \times 100\% \quad (6)$$

For clarification, (i = 2, 3, 4, 5, 6, …) is the ith harmonic-order amplitude and the parameter E_i depicts the fundamental value of the back-EMF.

Fig.8 depicts the waveform of the cogging torque of both topologies. Nonetheless, cogging-torque is inevitable in PM-designed motors and evolves as a result of the established interactions between the PMs configured in the rotor-topology and the laminated designed stator-slot-teeth [39-41].

Meanwhile, the computed peak-peak cogging torque for the URSTPM motor is lower than the MRSTPM motor. Although the MRSTPM motor's cogging torque is minimal compared to its output torque, it will not be a suitable design candidate for an application where minimal torque-ripple and acoustic noise is a key requirements compared to that of the URSTPM motor. Hence, the merits mentioned above make the URSTPM motor a promising candidate compared to the MRSTPM motor. To buttress the aforementioned point, the computed peak-to-peak cogging-torque values for the URSTPM motor and the MRSTPM motor are 367mNm and 498mNm, respectively.

4.2. Load Performance Analysis for the Two Topologies

This section of the research work considers the load-performance analysis of the aforementioned two designed spoke-type motors verified by the FEA of the ANSYS-Maxwell software at the rated current of 8.2Ampers. Meanwhile, Fig.9(a) depicts the output-torque waveform of both topologies. Nonetheless, it is imperative to highlight that the MRSTPM motor exhibits a slightly higher output torque as compared to the URSTPM motor. However, the computed output torque at the current angle of 0^0 for both the MRSTPM motor and URSTPM motor is 10.62Nm. and 9.65Nm, respectively.

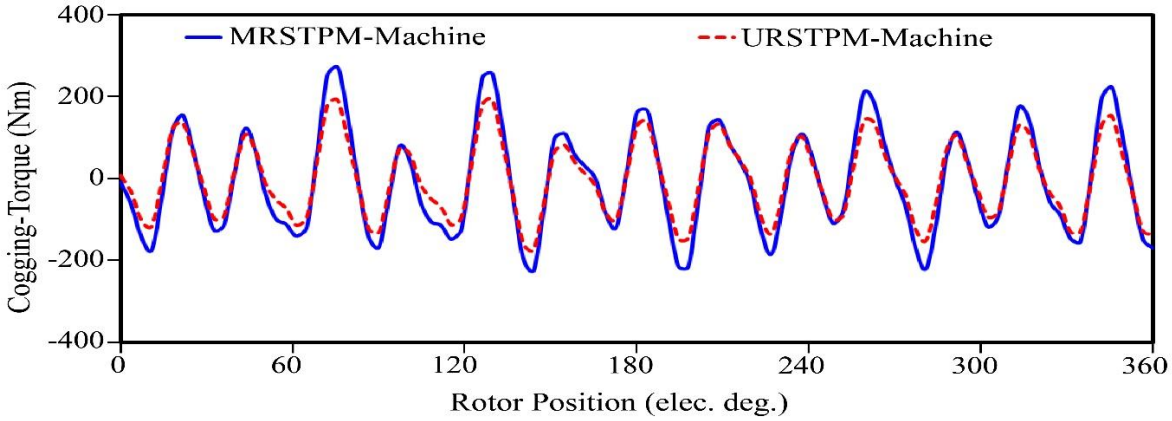

Fig. 8 Cogging-Torque Analysis of the spoke-type PM motors

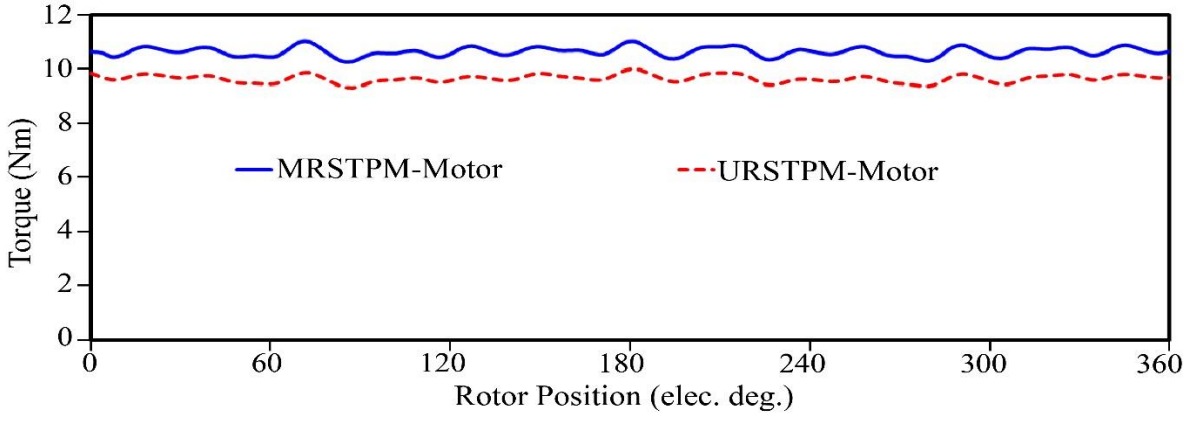

(a)

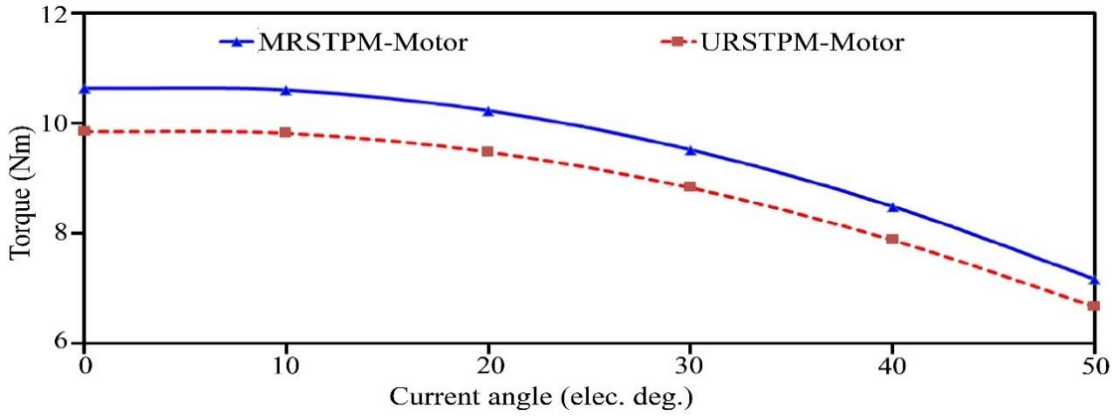

(b)

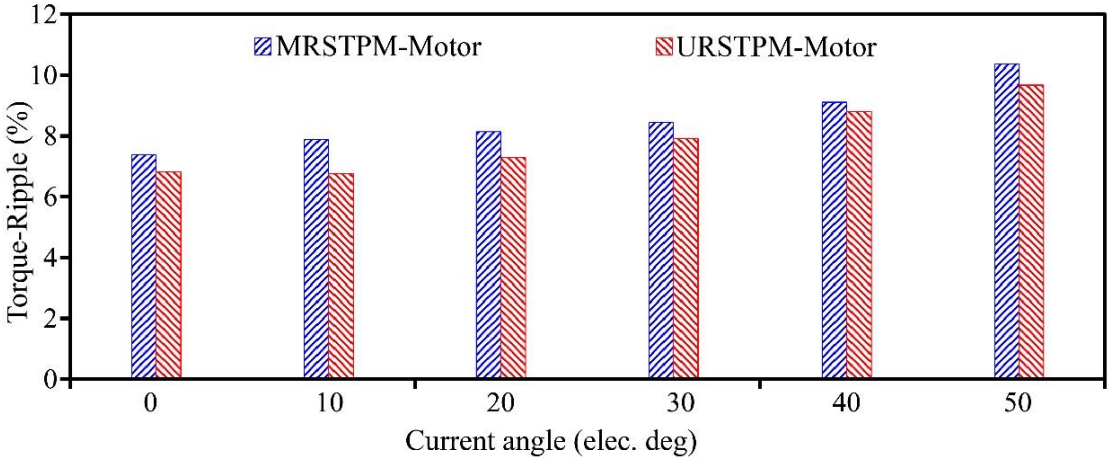

(c)

Fig. 9 Torque Analysis of the spoke-type PM motors. (a) Output-Torque- Waveform (b) Output-Torque at various Current-Angle Analysis (c) Torque-Ripple at various current-angles

Moreover, the estimated torque-ripple (T_{rip}) of the MRSTPM motor and URSTPM motor through (7) at the injected current angle of 0^o is 7.41% and 6.83%. Besides, Fig.9(b) presents the output torque at various or distinct current angles, with the MRSTPM motor exhibiting higher output torque at all the selected operating current angles compared to the URSTPM motor. Meanwhile, Fig. 9(c) shows the torque-ripple at various current-angle for both topologies. However, as presented in Fig.9 (c), the URSTPM-motor exhibit a minimal torque ripple compared to the MRSTPM motor.

$$T_{rip} = \frac{T_{p\text{-}p}}{T_{avg}} \times 100\% = \frac{(T_{\max}\text{-}T_{mim})}{T_{avg}} \times 100\% \quad (7)$$

4.3. Power-Density and Torque-Density Analysis for the Two Topologies

The design parameters, such as power density, torque density, and efficiency, are imperative in PM motors. Besides, the above-mentioned parameters play a key role in EV traction applications. Hence, this section compares the aforementioned design parameters for the MRSTPM motor and the URSTPM motor at the current angle of 0^0. The selected design specifications of the MRSTPM motor and URSTPM motors, such as the axial length and the stator-outer diameter, are 60mm and 145mm.

Besides, the verified output power at the current angle of 0^0 for both the MRSTPM motor and the URSTPM motor is 1.67*Kw* and 1.55*Kw*, respectively. Hence, this results in a motor volume of 0.99L for both motor topologies. However, the computed power density and torque density of the MRSTPM motor is 1.69 *Kw/L* and 10.73 *Nm/L*, respectively, while the power density and torque density of the URSTPM motor is 1.57 *kW* and 9.95 *Nm/L*, respectively.

Hence, from the aforementioned analysis, the power density and torque density of the MRSTPM motor is slightly higher than that of the URSTPM motor. Besides, for intuitive analysis of the aforementioned motor topologies, the computing power and torque densities with their corresponding design parameter specifications are presented in Table 3. Moreover, the efficiency of both topologies will be analyzed and compared in the next section.

Table 3. Power Density Comparison of the Two Spoke-Type Motors

Items	MRSTPM-Motor	URSTPM-Motor	%Decreased
Output Power (kW)	1.67	1.55	7.2
Axial-Length (mm)	60	60	-
Volume (L)	0.99	0.99	-
Power Density(kW/L)	1.69	1.57	7.1
Torque Density(Nm/L)	10.73	9.95	7.3

4.4. Losses and Efficiency Analysis for the Two Topologies

Electrical machines, especially, motor nearly consume or utilize 70 percent (70%) of the overall generated electrical energy globally. Moreover, operating efficiency and electrical energy control or management have engendered enormous concerns. Besides, research depicts that even one percent (1%) enhancement in the operating efficiency of an electric motor can inevitably save an enormous amount of energy (electricity) units per annum [42]. Hence, it is imperative to carefully consider the efficiency analysis of an electric motor during the initial design stage to minimize the amount of electric energy consumed by the electric motor to save energy.

The losses in an electrical motor have a significant effect on its efficiency. Meanwhile, electrical motor efficiency is one of the key components in EV traction applications. However, the considered losses in the two designed topologies are the stator-losses (ST-Losses), rotor-losses (RT-Losses), PM-Losses, and copper-losses (*Pcu*). Nonetheless, as presented in Fig.10 (a) to (c), the core, as mentioned above, and PM losses exhibited by the URSTPM motor are lower than that of the MRSTPM motor. Besides, the ST-loss, RT-loss, and PM-loss in the URSTPM motor exhibit 15.2%, 13.68%, and 51.59% reduction compared to the MRSTPM motor. Moreover, the computed P_{cu} for both topologies is the same. However, the computed losses are presented in Table 4 for intuitive analysis. Hence, from the above analysis, it can be predicted that the URSTPM motor can exhibit higher efficiency than the MRSTPM motor.

Table 4. Iron Loss Comparison of the Two Spoke-Type PM Motors

Items	MUSTPM-Motor	URSTPM-Motor	%Decreased
Stator iron loss (W)	81.63	69.23	15.2
Rotor iron loss (W)	3.07	2.65	13.68
PM loss(W)	2.19	1.06	51.59
Copper loss (W)	28.58	28.58	0

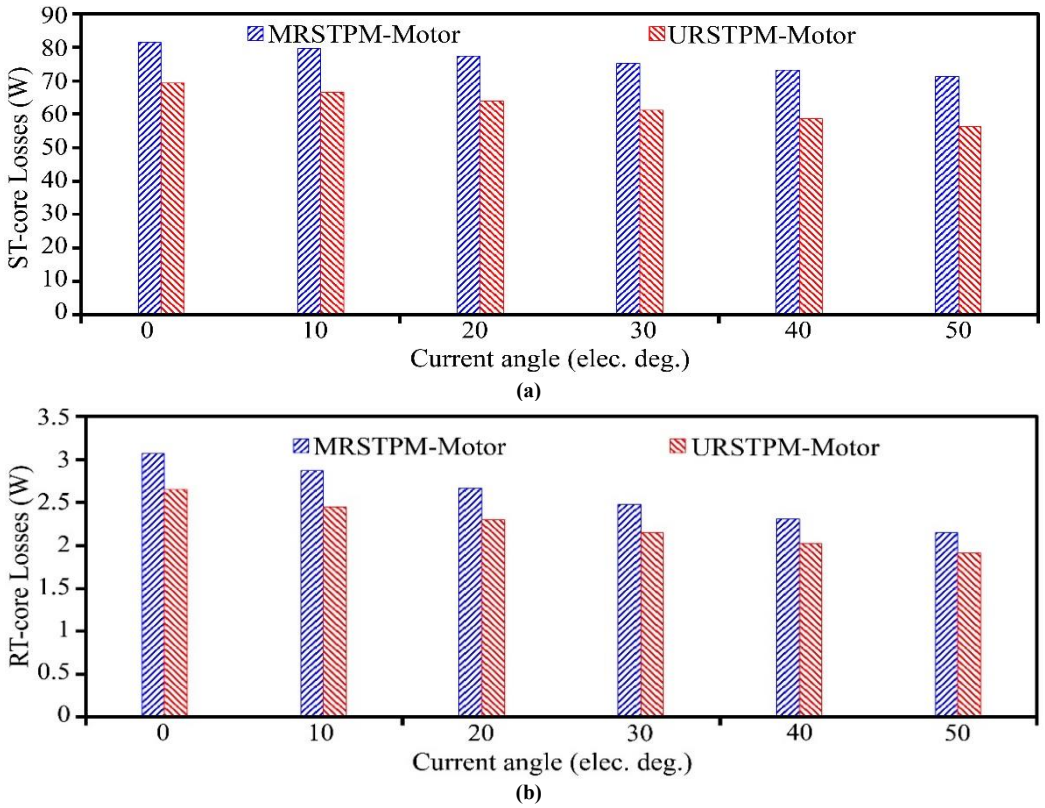

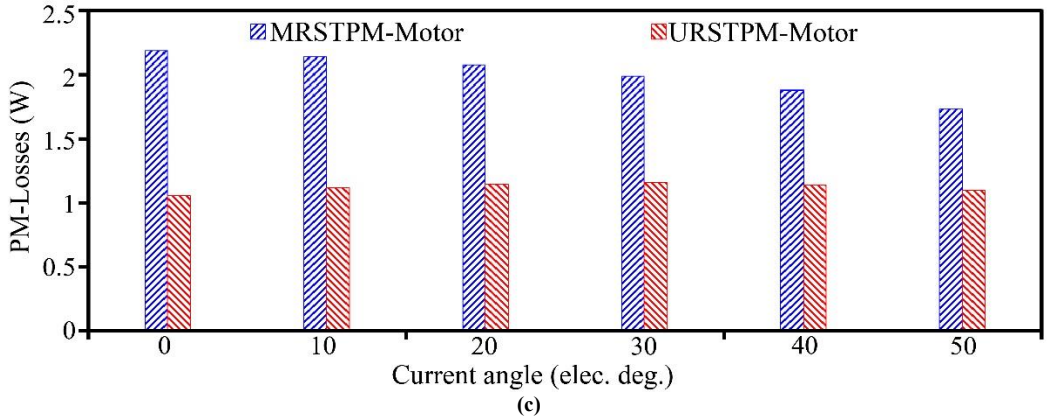

(c)

Fig. 10 Spoke-type PM motors Losses. (a) ST-Losses (b) RT-Losses (c) PM-Losses

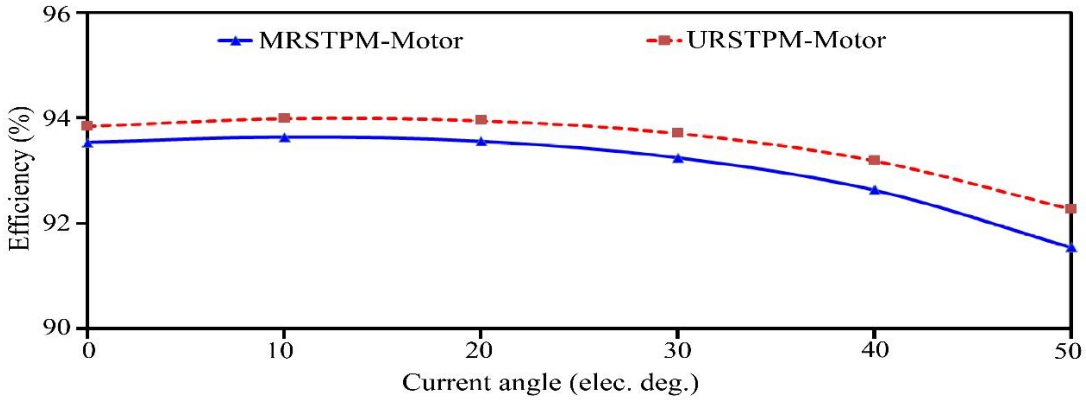

Fig. 11 Efficiency Analysis of the Spoke-type PM motors at various current-angle

Moreover, the estimated output power of both the MRSTPM motor and URSTPM motor at the current angle of 0° is 1.67*Kw* and 1.55*Kw*, respectively. Hence, from the aforementioned parameters, the efficiency of both topologies can be derived from (8).

$$\eta = \frac{T_{avg\omega}}{T_{avg\omega} + P_{FE} + P_{PM} + P_{CU}} \times 100\% \quad (8)$$

Where T_{avgw}, P_{FE}, $P_{PM,}$ and P_{cu} depict the output power, the core-losses (ST-Loss and RT-Loss), PM-Loss, and copper-loss, respectively. Therefore, the computed efficiency for the MRSTPM motor and the URSTPM motor at the current angle of 0° is 93.53% and 93.84%, respectively. Hence, the URSTPM motor unveils a slightly higher efficiency than the MRSTPM motor. To buttress the above-mentioned point, the efficiency of both topologies at distinct stipulated current angles is presented in Fig.11. Nonetheless, it can be seen in Fig.11 that the URSTPM motor exhibits slightly higher efficiency as compared to the MRSTPM motor at all the various current-angle.

4.5. Electrical-Loading and Heat-load Analysis for the Two Motor Topologies

The heat-loading of an electrical machine is key in determining the right cooling system for a particular motor. Meanwhile, the electrical loading (E_d) of both the MRSTPM motor and URSTPM motor can be deduced from (9).

$$E_d = \frac{2mNI}{\pi D_{si}} \quad (9)$$

Where the selected symbols, namely *N*, *m*, *I*, and D_{si} are the number of turns, the number of phases for the motors, the maximum current, and the inner stator diameter. Hence, the heat load can be computed by the product of E_d and the current density *J*. Besides, with the current density of 5.3/mm^2, the heat load of both topologies is 47.25A/mm^2. Since the calculated heat load is far less than 1000A/mm^3, a natural cooling system is appropriate for both spoke-type PM motors under consideration.

4.6. Fault-Tolerant Capacity Analysis for the Two Motor Topologies

The analysis of self-inductance and mutual inductance are key electric motor design parameters to evaluate the fault-tolerant capacity of the motor. Moreover, the mutual inductance in motor design is an imperative parameter to ascertain or prove the strength level of the electromagnetic coupling effect generated between the designated adjacent phases. Hence, it is essential to fine-tune or optimize the electric motor to ensure a minimal range of mutual inductance to guarantee sufficient independence of

designated motor phases whilst keeping a higher self-inductance level to limit short-circuit flow current during fault-condition. Howbeit, as illustrated via the waveforms depicted respectively in Fig. 12(a) and (b), the calculated mutual-inductance value via the finite element analysis (FEA) depicts that the URSTPM motor exhibit a lower level of mutual inductance compared to that of the MRSTPM motor, which is favorable for ensuring enhanced magnetic isolation of the design motor phases. Nonetheless, as presented in the waveform of Fig. 12(c), the URSTPM motor unveiled a higher value of phase self-inductance than that of the MRSTPM motor topology, which is worthy of or beneficial for limiting the flow of the short-circuit current in the event of fault-condition. Hence, from the aforementioned analysis, the URSTPM motor topology can unveil splendid fault-tolerant capacity in terms of winding fault conditions compared to the MRSTPM motor topology.

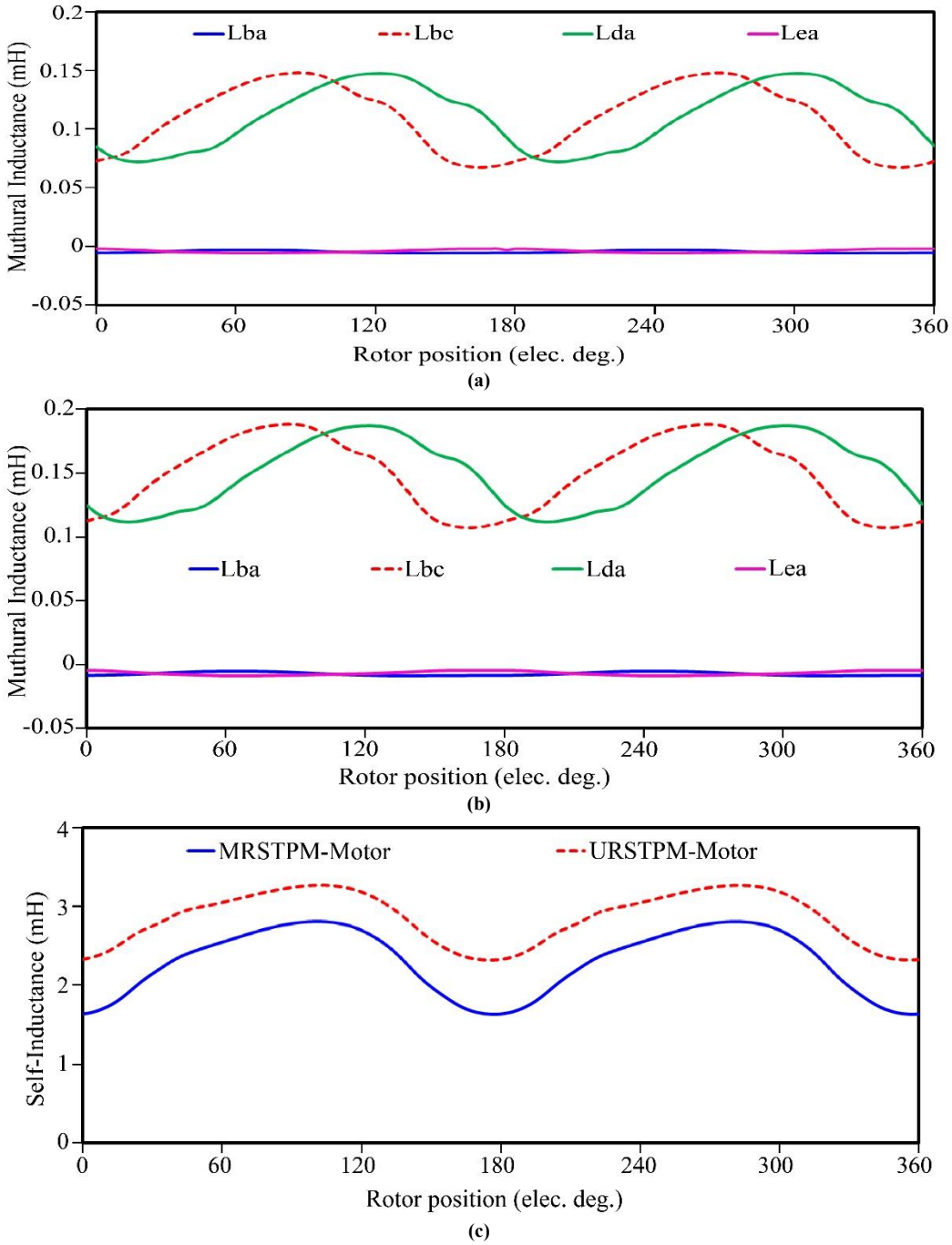

Fig. 12 Fault-tolerant Comparison of the Spoke-type PM motors (a) Mutual-inductance of URSTPM motor (b) Mutual-inductance of MRSTPM motor (c) Self-inductance of the two motors

5. Conclusion

In this research paper, a spoke-type PM motor with two distinctive rotors, a modular-rotor spoke-type PM (MRSTPM) motor and a union-rotor spoke-type PM (MRSTPM) motor are analyzed and compared for EV and HEV traction applications. Meanwhile, the electromagnetic performances of both topologies are verified by the FEA of the ANSYS-Maxwell software. However, the results unveil a comparable electromagnetic output performance for the MRSTPM motor and the URSTPM motor. Moreover, from the manufacturing point of view, the MRSTPM motor topology is complex due to its separate (modular) rotor core compared to the URSTPM motor with one complete (union) rotor core. Besides, the URSTPM motor exhibits slightly higher efficiency with reduced cogging-torque, torque-ripple, and motor losses compared to the MRSTPM motor. Albeit the MRSTPM motor exhibits a slightly higher electromagnetic output torque compared to the URSTPM motor, the URSTPM motor is selected as the preferred and promising candidate for EV traction applications due to the demerits of reduced operating efficiency as a result of high motor losses with higher cogging-torque, higher torque-ripple, and manufacturing complexity of the rotor-topology in the MRSTPM-motor.

References

[1] C. C. Chan, "The State of the Art of Electric and Hybrid Vehicles," *Proceedings of the IEEE,* vol. 90, no. 2, pp. 247-275, 2002. *Crossref,* http://doi.org/10.1109/5.989873

[2] Ping Zheng et al., "Investigation of a Five-Phase 20-Slot/18-Pole PMSM for Electric Vehicles," *International Conference on Electrical Machines and Systems,* pp. 1168-1172, 2014. *Crossref,* http://doi.org/10.1109/ICEMS.2014.7013664

[3] K. T. Chau, C. C. Chan, and Chunhua Liu, "Overview of Permanent-Magnet Brushless Drives for Electric and Hybrid Electric Vehicles," *IEEE Transactions on Industrial Electronics,* vol. 55, no. 6, pp. 2246-2257, 2008. *Crossref,* http://doi.org/10.1109/TIE.2008.918403

[4] T. Gundogdu, Z. Q. Zhu, and J. C. Mipo, "Optimization and Improvement of Advanced Nonoverlapping Induction Machines for EVs/HEVs," *IEEE Access,* vol. 10, pp. 13329-13353, 2022. *Crossref,* http://doi.org/10.1109/ACCESS.2022.3148246

[5] X. Liu et al., "Efficiency Improvement of Switched Flux PM Memory Machine Over Interior PM Machine for EV/HEV Applications," *IEEE Transactions on Magnetics,* vol. 50, no. 11, pp. 1-4, 2014. *Crossref,* http://doi.org/10.1109/TMAG.2014.2323556

[6] Qian Chen et al., "A New Fault-Tolerant Permanent-Magnet Machine for Electric Vehicle Applications," *IEEE Transactions on Magnetics,* vol. 47, no. 10, pp. 4183-4186, 2011. *Crossref,* http://doi.org/10.1109/TMAG.2011.2146238

[7] Wenxiang Zhao et al., "Remedial Brushless AC Operation of Fault-Tolerant Doubly Salient Permanent-Magnet Motor Drives," *IEEE Transactions on Industrial Electronics,* vol. 57, no. 6, pp. 2134-2141, 2010. *Crossref,* http://doi.org/10.1109/TIE.2009.2033824

[8] Jiangui Li et al., "A New Efficient Permanent-Magnet Vernier Machine for Wind Power Generation," *IEEE Transactions on Magnetics,* vol. 46, no. 6, pp. 1475-1478, 2010. *Crossref,* http://doi.org/10.1109/TMAG.2010.2044636

[9] David G. Dorrell et al., "Comparison of Different Motor Design Drives for Hybrid Electric Vehicles," *IEEE Energy Conversion Congress and Exposition, Atlanta, GA, USA*, pp. 3352-3359, 2010. *Crossref,* http://doi.org/10.1109/ECCE.2010.5618318

[10] Akira Chiba et al., "Torque Density and Efficiency Improvements of a Switched Reluctance Motor Without Rare-Earth Material for Hybrid Vehicles," *IEEE Transactions on Industry Applications,* vol. 47, no. 3, pp. 1240-1246, 2011. *Crossref,* http://doi.org/10.1109/TIA.2011.2125770

[11] Z. Q. Zhu et al., "Comparative Study of Partitioned Stator Machines with Different PM Excitation Stators," *IEEE Transactions on Industry Applications,* vol. 52, no. 1, pp. 199-208, 2016. *Crossref,* http://doi.org/10.1109/TIA.2015.2477055

[12] Z. Q. Zhu, and D. Howe, "Electrical Machines and Drives for Electric, Hybrid, and Fuel Cell Vehicles," *Proceedings of the IEEE,* vol. 95, no. 4, pp. 746-765, 2007. *Crossref,* http://doi.org/10.1109/JPROC.2006.892482

[13] Wenxiang Zhao et al., "Star and Delta Hybrid Connection of an FSCW PM Machine for Low Space Harmonics," *IEEE Transactions on Industrial Electronics,* vol. 65, no. 12, pp. 9266-9279, 2018. *Crossref,* http://doi.org/10.1109/TIE.2018.2807365

[14] Wenxiang Zhao et al., "Design and Analysis of a Linear Permanent-Magnet Vernier Machine with Improved Force Density," *IEEE Transactions on Industrial Electronics,* vol. 63, no. 4, pp. 2072-2082, 2016. *Crossref,* http://doi.org/10.1109/TIE.2015.2499165

[15] Shushu Zhu et al., "Iron Loss and Efficiency Analysis of Interior PM Machines for Electric Vehicle Applications," *IEEE Transactions on Industrial Electronics,* vol. 65, no. 1, pp. 114-124, 2018. *Crossref,* http://doi.org/10.1109/TIE.2017.2723859

[16] Qian Chen et al., "A Novel Spoke-Type PM Motor with Auxiliary Salient Poles for Low Torque Pulsation," *IEEE Transactions on Industrial Electronics,* vol. 67, no. 6, pp. 4762-4773, 2020. *Crossref,* http://doi.org/10.1109/TIE.2019.2924864

[17] Sung Gu Lee, Jaenam Bae, and Won-Ho Kim, "A Study on the Maximum Flux Linkage and the Goodness Factor for the Spoke-Type PMSM," *IEEE Transactions on Applied Superconductivity,* vol. 28, no. 3, pp. 1-5, 2018. *Crossref,* http://doi.org/10.1109/TASC.2017.2775561

[18] Xiang Ren et al., "Investigation of Spoke Array Permanent Magnet Vernier Machine with Alternate Flux Bridges," *IEEE Transactions on Energy Conversion,* vol. 33, no. 4, pp. 2112-2121, 2018. *Crossref,* http://doi.org/10.1109/TEC.2018.2846259

[19] Le Sun et al., "Key Issues in Design and Manufacture of the Magnetic-Geared Dual-Rotor Motor for Hybrid Vehicles," *IEEE Transactions on Energy Conversion,* vol. 32, no. 4, pp. 1492-1501, 2017. *Crossref,* http://doi.org/10.1109/TEC.2017.2697758

[20] K. Y. Hwang, J. H. Jo, and B. I. Kwon, "A Study on Optimal Pole Design of Spoke-Type IPMSM with a Concentrated Winding for Reducing the Torque Ripple by Experiment Design Method," *IEEE Transactions on Magnetics,* vol. 45, no. 10, pp. 4712-4715, 2009. *Crossref,* http://doi.org/10.1109/TMAG.2009.2022645

[21] Pham Van Tuan et al., "Direct Torque Control of an Interior Permanent Magnet Synchronous Motor," *SSRG International Journal of Electrical and Electronics Engineering,* vol. 9, no. 7, pp. 1-5, 2022. *Crossref,* https://doi.org/10.14445/23488379/IJEEE-V9I7P101

[22] Peng Su et al., "Analysis of Stator Slots and Rotor Pole Pairs Combinations of Rotor-Permanent Magnet Flux-Switching Machines," *IEEE Transactions on Industrial Electronics,* vol. 67, no. 2, pp. 906-918, 2020. *Crossref,* https://doi.org/10.1109/TIE.2019.2901653

[23] Xiaoyong Zhu et al., "Co-Reduction of Torque Ripple for Outer Rotor Flux-Switching PM Motor Using Systematic Multi-Level Design and Control Schemes," *IEEE Transactions on Industrial Electronics,* vol. 64, no. 2, pp. 1102-1112, 2017. *Crossref,* https://doi.org/10.1109/TIE.2016.2613058

[24] Chunhua Liu, "Emerging Electric Machines and Drives — An Overview," *IEEE Transactions on Energy Conversion,* vol. 33, no. 4, pp. 2270-2280, 2018. *Crossref,* https://doi.org/10.1109/TEC.2018.2852732

[25] A.G. Jack, B.C. Mecrow, and J.A. Haylock, "A Comparative Study of Permanent Magnet and Switched Reluctance Motors for High-Performance Fault-Tolerant Applications," *IEEE Transactions on Industry Applications,* vol. 32, no. 4, pp. 889-895, 1996. *Crossref,* https://doi.org/10.1109/28.511646

[26] E. Richter et al., "An Integrated Electrical Starter/Generator System for Gas Turbine Application, Design and Test Results," *Proceedings of ICEM Conference,* 1994.

[27] E. Richter, "Switched Reluctance Machines for High-Performance Operations in a Harsh Environment - A Review Paper," *Proceedings of ICEM Conference, Boston,* vol. 1, pp. 18-24, 1990.

[28] Eike Richter, "High Temperature Switched Reluctance Motors and Generators for Future Aircraft Engine Applications," *Proceedings of American Control Conference, Atlanta,* pp. 1846-1851, 1988. *Crossref,* https://doi.org/10.23919/ACC.1988.4790027

[29] C. M. Stephens, "Fault Detection and Management System for Fault-Tolerant Switched Reluctance Motor Drives," *IEEE Transactions on Industry Applications,* vol. 27, no. 6, pp. 1098-1102, 1991. *Crossref,* https://doi.org/10.1109/28.108460

[30] C.A. Ferreira et al., "Design and Implementation of a Five-Hp, Switched Reluctance, Fuel-Lube, Pump Motor Drive for a Gas Turbine Engine," *IEEE Transactions on Power Electronics*, vol. 10, no. 1, pp. 55-61, 1995. *Crossref,* https://doi.org/10.1109/63.368460

[31] Stephen Eduku et al., "A New Fault-Tolerant Rotor Permanent Magnet Flux-Switching Motor," *IEEE Transactions on Transportation Electrification,* vol. 8, no. 3, pp. 3606-3617, 2022. *Crossref,* https://doi.org/10.1109/TTE.2022.3143097

[32] A.J. Mitcham, G. Antonopoulos, and J.J.A. Cullen, "Favourable Slot and Pole Number Combinations for Fault-Tolerant PM Machines," *IEEE Proceedings - Electric Power Applications,* vol. 151, no. 5 pp. 520-525, 2004. *Crossref,* https://doi.org/10.1049/ip-epa:20040584

[33] A. S. Abdel-Khalik, "Five-Phase Modular External Rotor PM Machines with Different Rotor Poles: A Comparative Simulation Study," *Modeling and Simulation in Engineering,* 2012. *Crossref,* https://doi.org/10.1155/2012/487203

[34] Enrico Carraro et al., "Performance Comparison of Fractional Slot Concentrated Winding Spoke Type Synchronous Motors with Different Slot-Pole Combinations," *IEEE Energy Conversion Congress and Exposition,* pp. 6067-6074, 2015. *Crossref,* https://doi.org/10.1109/ECCE.2015.7310510

[35] Yi Sui et al., "Research on a 20-Slot/22-Pole Five-Phase Fault-Tolerant PMSM Used for Four-Wheel-Drive Electric Vehicles," *Energies,* vol. 7, no. 3, pp. 1265-1287, 2014. *Crossref,* https://doi.org/10.3390/en7031265

[36] Chengde Tong et al., "Analysis and Design of a Fault-Tolerant Six-Phase Permanent-Magnet Synchronous Machine For Electric Vehicles," *17th International Conference on Electrical Machines and Systems (ICEMS),* pp. 1629-1632, 2014. *Crossref,* https://doi.org/10.1109/ICEMS.2014.7013738

[37] Li Zhang et al., "Design and Analysis of a New Six-Phase Fault-Tolerant Hybrid-Excitation Motor for Electric Vehicles," *IEEE Transactions on Magnetics,* vol. 51, no. 11, pp. 1-4, 2015. *Crossref,* https://doi.org/10.1109/TMAG.2015.2447276.

[38] Ping Zheng et al., "Investigation of a Novel 24-Slot/14-Pole Six-Phase Fault-Tolerant Modular Permanent-Magnet In-Wheel Motor for Electric Vehicles," *Energies,* vol. 6, no. 10, pp. 4980-5002, 2013. *Crossref,* https://doi.org/10.3390/en6104980

[39] Z. Q. Zhu, Z. Z. Wu, and X. Liu, "A Partitioned Stator Variable Flux Reluctance Machine," *IEEE Transactions on Energy Conversion,* vol. 31, no. 1, pp. 78-92, 2016. *Crossref,* https://doi.org/10.1109/TEC.2015.2470122.

[40] N. Bianchi, and S. Bolognani, "Design Techniques for Reducing the Cogging Torque in Surface-Mounted PM Motors," *IEEE Transactions on Industry Applications,* vol. 38, no. 5, pp. 1259-1265, 2002. *Crossref,* https://doi.org/10.1109/TIA.2002.802989

[41] Li Zhu et al., "Analytical Methods for Minimizing Cogging Torque in Permanent-Magnet Machines," *IEEE Transactions on Magnetics,* vol. 45, no. 4, pp. 2023-2031, 2009. *Crossref,* https://doi.org/10.1109/TMAG.2008.2011363

[42] Tejas H. Panchal, Rajesh M. Patel, and Amit N. Patel, "Efficiency Improvement of Radial Flux Permanent Magnet Brushless DC Motor Using Hiperco Magnetic Material," *International Journal of Engineering Trends and Technology*, vol. 60, no. 5, pp. 57-61, 2021. *Crossref*, https://doi.org/10.14445/22315381/IJETT-V69I5P210

[43] D. Y. Kim, J. K. Nam, and G. H. Jang, "Reduction of Magnetically Induced Vibration of a Spoke-Type IPM Motor Using Magneto-Mechanical Coupled Analysis and Optimization," *IEEE Transactions on Magnetics*, vol. 49, no. 9, pp. 5097-5105, 2013. *Crossref*, https://doi.org/10.1109/TMAG.2013.2255307